Reconstruction of the time profile of 20.35 GeV, subpicosecond long electron bunches by means of coherent Smith-Purcell radiation

H. L. Andrews,[1] F. Bakkali Taheri,[2] J. Barros,[4] R. Bartolini,[2] V. Bharadwaj,[3] C. Clarke,[3] N. Delerue,[4] G. Doucas,[2,*] N. Fuster-Martinez,[5] M. Vieille-Grosjean,[4] I. V. Konoplev,[2] M. Labat,[6] S. Le Corre,[4] C. Perry,[2] A. Reichold,[2] and S. Stevenson[2]

[1]*LANL, Los Alamos, New Mexico 87545, USA*
[2]*The John Adams Institute, Department of Physics, University of Oxford, Oxford OX1 3RH, United Kingdom*
[3]*SLAC National Accelerator Laboratory, Stanford, California 94025, USA*
[4]*LAL, CNRS and Universite Paris-Sud, 91898 Orsay, France*
[5]*Instituto de Física Corpuscular, IFIC (CSIC-UV), Valencia 46980, Spain*
[6]*Synchrotron SOLEIL, Saint-Aubin 91190, France*

(Received 22 November 2013; published 27 May 2014)

We have used coherent Smith-Purcell radiation (cSPr) in order to determine the temporal profile of sub-ps long electron bunches at the Facility for Advanced Accelerator Experimental Tests, at SLAC. The measurements reported here were carried out in June 2012 and April 2013. The rms values for the bunch length varied between 356 to 604 fs, depending on the accelerator settings. The resolution of the system was limited by the range of detectable wavelengths which was, in turn, determined by the choice of the grating periods used in these experiments and the achievable beam-grating separation. The paper gives the details of the various steps in the reconstruction of the time profile and discusses possible improvements to the resolution. We also present initial measurements of the polarization properties of cSPr and of the background radiation.

DOI: 10.1103/PhysRevSTAB.17.052802 PACS numbers: 41.60.-m, 41.85.Ew, 41.75.Ht

I. INTRODUCTION

The past few years have seen considerable activity, and significant progress, in the field of plasma wakefield acceleration [1–3]. The electron bunches generated in a plasma which is excited either by a "drive" electron beam or by a laser, can be as short as a few tens of fs and their repetition rate and shot-to-shot stability are likely to be low. This requires a new generation of beam diagnostic tools, especially for the determination of the temporal profile of the bunch. The ultimate objective of the present work is the development of a device that can achieve this in a single shot and in a nondestructive manner. The experimental arrangement described in the present paper does not have single-shot capability but it has provided useful information for the eventual design of a true "single-shot" bunch profile monitor. Although there are other nondestructive methods capable of achieving single-shot performance [4,5], cSPr offers particularly good prospects in this respect: (a) it has true single-shot capability, in the sense that *one and the same bunch* can provide all the information in the frequency domain that is needed for the reconstruction of the bunch profile; (b) there is no need for an external spectrometer; (c) wide frequency coverage through the use of multiple gratings; and (d) much stronger signal compared with diffraction radiation; the grating is an array of N (number of periods) equal oscillators and, hence, the intensity is increased by N^2.

A. Overview of coherent Smith-Purcell radiation

When any charged particle (in our case an electron) is traveling with velocity βc, where c is the speed of light, at a height x_0 above the surface of a metallic grating of period l, radiation is emitted from the surface of the grating; this is known as Smith-Purcell radiation. A number of theories have been proposed in order to describe the origin of this radiation; brief summaries and references can be found in [6–8]. In the present paper we follow the "surface current" theory whereby the radiation arises from the acceleration of the charges induced on the surface of the grating by the traveling electron. The details of this theory have been given in [9,10] and, therefore, we restrict the discussion to a few essential points. The grating disperses the radiation and the relationship between the emitted wavelength (λ), the observation angle (θ) and the electron velocity (β), expressed as a fraction of the speed of light, is given by

*Corresponding author.
g.doucas@physics.ox.ac.uk

$$\lambda = \frac{l}{n}\left(\frac{1}{\beta} - \cos\theta\right), \tag{1}$$

where n is the order of emission. The axes convention used in this paper is shown in Fig. 1: the electron is traveling in the z direction, the perpendicular to the grating surface is along the x axis and the grooves of the grating are along the y direction. The observation angle θ is the angle between the position vector of the observer ($\bar{n}$) and the z axis, while the azimuthal angle (ϕ) is the angle between the projection of $\bar{n}$ into the x-y plane and the positive x axis. It is defined to be zero when $\bar{n}$ is in the x-z plane. The origin of the coordinate system is assumed to be at the center of the grating. Expression (1) is valid if the observation is taking place in the x-z plane ($\phi = 0$) and the observer is at "infinity," in which case the radiation is essentially monochromatic at a given observation point, with a relative linewidth $\mathrm{d}\lambda/\lambda = 1/(nN)$ and thus determined by the number (N) of grating periods and the order n of the radiation.

It can be shown [9] that the energy dI emitted per unit solid angle $d\Omega$ by a single electron (the single-electron yield) passing at a distance x_0 above the grating, is given by

$$\left(\frac{dI}{d\Omega}\right)_1 = 2\pi e^2 \frac{Z}{l^2}\frac{n^2\beta^3}{(1-\beta\cos\theta)^3}R^2. \tag{2}$$

In the above expression Z is the length of the grating, e is the electron charge (in CGS units) and R^2 is a function of the electron-grating separation (x_0), the grating profile, the emission angle and the order of the radiation. R^2 has to be calculated numerically. In the idealized case of a grating of infinite width, the dependence of the yield on x_0 can be separated out of the R^2 term and is contained only in the exponential term of Eq. (2a):

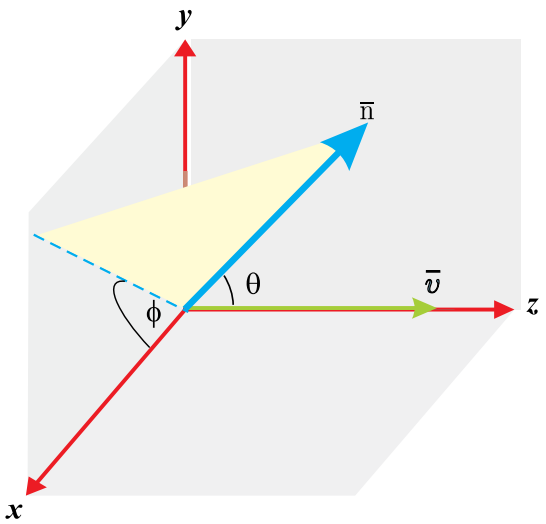

FIG. 1. Schematic of the axes convention.

$$\left(\frac{dI}{d\Omega}\right)_1 = 2\pi e^2 \frac{Z}{l^2}\frac{n^2\beta^3}{(1-\beta\cos\theta)^3}\exp\left[-\frac{2x_0}{\lambda_e}\right]R_\infty^2. \tag{2a}$$

The new term R_∞^2 is now independent of the beam-grating separation. The quantity λ_e in (2a) is a measure of the beam-grating coupling efficiency, known as the "evanescent wavelength" and defined by

$$\lambda_e = \frac{\beta\gamma\lambda}{2\pi\sqrt{1+\beta^2\gamma^2\sin^2\theta\sin^2\varphi}}. \tag{3}$$

In the present paper the *finite* width of the grating has been taken into account and the single-electron yield has been calculated from expression (2).

In the case of a bunch consisting of N_e electrons, the emitted energy per solid angle is given by the expression

$$\left(\frac{dI}{d\Omega}\right)_{N_e} = \left(\frac{dI}{d\Omega}\right)_1 (N_e S_{\mathrm{inc}} + N_e^2 S_{\mathrm{coh}}). \tag{4}$$

This expression is applicable to all radiative processes induced by electron beams and the dimensionless quantities S_{coh} and S_{inc} describe the way in which the contributions of individual electrons in the bunch add up to the total intensity. If the bunch is short compared with the observed wavelength, the first term in the parentheses on the right-hand side is negligible compared with the second and the yield is proportional to the square of the number of electrons. This is the "coherent" regime and its onset occurs, approximately, when the bunch length is equal to the wavelength. Conversely, in the case of a very long bunch (or DC beam) the 2nd term is negligible, the radiation becomes "incoherent" and the total yield is just proportional to the number of electrons. Since the range of emitted wavelengths is determined by the period of the grating, a suitable choice of its period can bring the emission into the coherent regime [see Eq. (1)]. Coherent emission is of interest, not only because of the enormous increase in yield but, also, because it offers a way of recovering the time profile of the bunch, as discussed below.

Assuming that the charge distribution $q(x, y, t)$ in the bunch can be expressed as

$$q(x, y, t) = X(x)Y(y)T(t)$$

and that the bunch is traveling along the center line of the grating ($y = 0$), the incoherent and coherent integrals S_{coh} and S_{inc} in (4) are given by

$$S_{\mathrm{inc}} \propto \int_0^\infty XR^2 dx$$

and

$$S_{\mathrm{coh}} \propto \left| \int_0^\infty XRdx \right|^2 \left| \int_{-\infty}^\infty Ye^{-ik_y}dy \right|^2 \left| \int_{-\infty}^\infty Te^{-i\omega t}dt \right|^2$$

respectively.

In the above expressions, ω is the angular frequency of the radiation and $k_y = k\sin\theta\sin\phi$ is the y component of its wave vector ($\bar{k}$). Of the three integrals in the expression for S_{coh}, the first two describe the effect of the transverse dimensions of the bunch, while the third integral, which is the squared modulus of the Fourier transform (FT) of the time profile of the bunch, can be used to reconstruct its temporal profile. Since the X and Y distributions are assumed to be known from independent measurements and the single electron yield can be calculated numerically, the following expressions,

$$\left(\frac{dI}{d\Omega}\right)_{N_e} \cong \left(\frac{dI}{d\Omega}\right)_1 N_e^2 S_{\mathrm{coh}} \approx \left(\frac{dI}{d\Omega}\right)_1 N_e^2 \left| \int_{-\infty}^\infty Te^{-i\omega t}dt \right|^2,$$

$$\text{and setting} \left| \int_{-\infty}^\infty Te^{-i\omega t}dt \right|^2 \equiv \rho^2(\nu), \quad \text{where } \nu = 2\pi/\omega$$

$$\left(\frac{dI}{d\Omega}\right)_{N_e} \cong \left(\frac{dI}{d\Omega}\right)_1 N_e^2 \rho^2(\nu), \tag{5}$$

can be used to calculate the magnitude (ρ) of the FT from the measured spectral yields of cSPr.

The rest of the paper is structured as follows: Section II deals with the experimental arrangement; Sec. III is a detailed description of the analysis procedure; Sec. IV presents results on the properties of the background (i.e., the non-cSPr) radiation and a preliminary investigation of the polarization of the SP signal; Sec. V discusses some of the reconstructed bunch profiles and Sec. VI presents the conclusions of this work and suggests future measurements.

II. EXPERIMENTAL

The Facility for Advanced Accelerator Experimental Tests (FACET) facility uses the first 2/3 of the SLAC accelerator to deliver electron beams whose energy (for the experiments reported here) was 20.35 GeV. The bunch train structure consists of a single bunch at a repetition rate of up to 10 Hz. The number of electrons per bunch was in the range 1.5–2.0 $\times 10^{10}$ during the June 2012 runs and 5–7 $\times 10^9$ in the April 2013 ones. The normalized beam emittance is estimated to have been about 60 mm-mrad. The beam charge, emittance and transverse dimensions were obtained from the accelerator control system; charge and position were monitored on a shot-to-shot basis. The beam size was measured with wire scanners.

The experimental apparatus consists of two basic units: (a) a vacuum chamber which contains the gratings and (b) the optical system, which is located outside the chamber and is used for the collection, filtering and detection of the far infrared (FIR) radiation. Since the overall arrangement is very similar to that described in [7], we concentrate only on important modifications and details.

A. The vacuum chamber

The chamber was designed to allow simultaneous measurement of the SP radiation at eleven observation angles relative to the beam direction, ranging from 40° to 140° in steps of 10°. The emitted radiation emerged from the chamber through eleven windows, one for each observation angle (see Fig. 2). Each window consisted of a 21 mm diameter disk of high resistivity crystalline silicon, 2.0 mm thick.

The chamber contains a remotely operated "grating carousel" with four positions. The first three positions were occupied by gratings and the fourth by a flat piece of metal which is referred to as the "blank." The blank is an exact replica of the gratings, apart from the absence of corrugations on its surface. The purpose of the blank is to provide a measure of the background radiation, i.e., of the radiation whose origin is not due to the corrugations of a grating surface (see Sec. IV).

Three different gratings with periods of 0.25, 0.5, and 1.0 mm were used in the June 2012 experiments, while in April 2013 the chosen periods were 0.05, 0.25, and 1.5 mm. The period of each grating consisted of two facets. The blaze angle of the first (upstream) facet, which is the angle between the facet and the beam direction (z), was 40° and 35° for the 0.5 and 1.0 mm gratings, respectively; all the other gratings had a blaze angle of 30°. The second facet was perpendicular to the first. The choice of blaze angle does affect the efficiency of the grating but no detailed study of this parameter was carried out and the angles chosen are not necessarily optimal. The gratings and the blank were made of aluminum and were 40 mm long, 20 mm wide, and 5 mm thick. The orientation of the

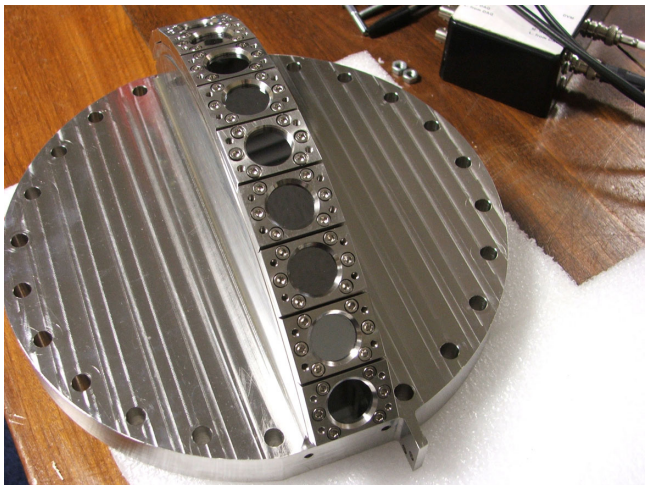

FIG. 2. Photograph of the chamber flange with the 11 silicon windows.

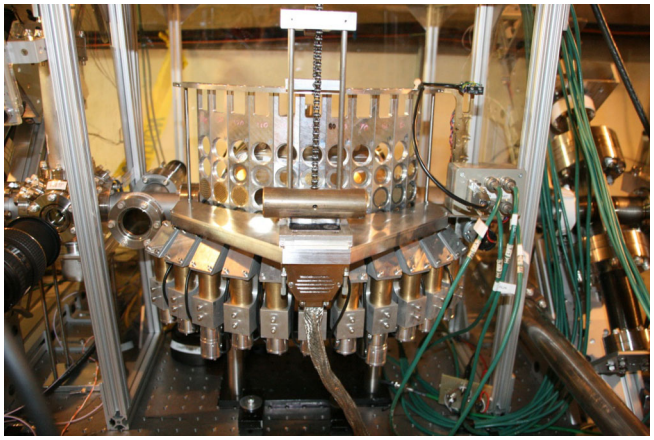

FIG. 3. The apparatus installed on the FACET beam line. Three of the filter rows are visible in the upper part of the filter ladder, together with the Winston cone-detector assemblies in the lower part of the photograph.

chamber in the beam line is such that the vertical to the grating surface coincides with the horizontal (x) direction. A remotely operated motor allowed the selected grating (or the blank) to move along the x axis and to be brought to the desired position, close to the beam centroid. The grating position was determined by means of a ten-turn potentiometer connected to the lead screw of the drive mechanism. Care was taken to survey the chamber and the grating mechanism at various grating positions, in conjunction with the potentiometer readings, in order to determine the position of the grating relative to the axis of the chamber to an accuracy of better than 0.1 mm. The chamber axis has been surveyed with respect to the ideal beam axis with an accuracy of 0.2 mm.

The beam-grating separation is determined from the grating position inside the vacuum chamber and from the position of the beam relative to the ideal beam axis. The former was derived from the potentiometer readings while the latter can be measured using beam position monitors (BPMs) upstream and downstream of the chamber. Their readings were interpolated to the SPR chamber location using a linear beam optics code. Unfortunately, the relative positions of the BPM's electric and geometric centers are uncertain to at least 0.5 mm. This is assumed to be the systematic uncertainty in the determination of the beam-grating separation.

The E203 apparatus has a total insertion length of about 0.6 m and is shown in Fig. 3 as installed in the FACET beam line.

B. The optical system

The main elements of the FIR detection system are the filters, the light concentrators (Winston cones), the pyroelectric detectors and the data acquisition system (DAQ).

Each grating is associated with a specific set of eleven filters whose transmission properties have been designed to match the range of wavelengths that are expected to impinge on it. The use of filters is necessary in order to reduce the background radiation which appears to cover a broad spectral range (see Sec. IV). Four different types of filter were used, depending on the desired wavelength range: thin film coated silicon or Mylar, wire mesh and waveguide array plate (WAP) filters. Most of the filters were of the WAP type. Each change of grating must be accompanied by a change of filters. This is done by another remotely controlled mechanism that can raise or lower the screen that carries the filters until the correct set is in place (see Fig. 3). The filter ladders had two additional sets of holes that could either be left empty, so that one could record the intensity of the unfiltered radiation, or could be fitted with wire polarizers, if required.

After the filter, the radiation is reflected onto the entrance aperture of a light concentrator (Winston cone) and is detected by means of room temperature pyroelectric detectors located 0.5 mm beyond the exit of the cone. There are thus, 11 cones and detectors, one per channel. These can be seen in Fig. 3 and their details, together with those of the data acquisition system (DAQ), can be found in [7].

III. ANALYSIS

A. General comments

It is useful to list at the outset the basic assumptions used in the analysis, together with a brief discussion of their implications.

1. The net SP signal is assumed to be the difference between the signal obtained from a grating minus that from the blank, observed through the same set of filters, under the same beam conditions and with both grating and blank positioned at the same distance from the beam; in other words, SPR is the increase in signal due to the introduction of corrugations on the surface of a blank piece of metal (see Sec. IV for details).

2. The charge distribution $q(x, y, t)$ in the bunch can be expressed by three uncorrelated distribution functions, i.e., $q(x, y, t) = X(x)Y(y)T(t)$ and moreover, the transverse distributions $X(x), Y(y)$ are assumed to be Gaussian. It is difficult to calculate analytically or test experimentally the effect of correlated charge distributions and we are not aware of any such measurements. However, for a well-focused beam the effect of the transverse distribution is likely to be small (see e.g., Ref. [11]) and the dominant influence will be that of the longitudinal distribution. The assumption of approximately Gaussian transverse distributions is supported by wire scanner measurements of the transverse beam profile.

3. Since the detectors are not located at infinity relative to the grating, the energy impinging on each detector is not concentrated in a single wavelength but is distributed over a band of wavelengths around the central wavelength of Eq. (1). This effect can be accounted for by an additional

"transmission" factor which has been calculated as follows, using a simple geometric construction: the grating can be considered as a series of N independent oscillators (N is the number of periods), excited sequentially by the beam. One period of the grating constitutes a single oscillator. For a given detector position and wavelength, it is easy to calculate the path differences between the detector and the oscillators and to compare this path length difference to the wavelength. This gives the phase of each oscillator relative to a reference phase, say that of the oscillator at the center of the grating. The contributions of all N oscillators, each with the appropriate phase, are then added and the resultant intensity is compared to that expected when all oscillators are in phase, i.e., when the detector is at infinity. The ratio of the two intensities is the transmission factor, whose values are listed in the Appendix.

4. We assume that the background radiation is beam induced (as opposed to, say, machine harmonics etc.). Hence, the background radiation must also be coherent. If the grating and blank signals are measured with different bunch charge, the charge correction is $\sim q^2$. In all the measurements reported here the charge variations over the time period required for one set of measurements (approximately ½ hour) were small (<5%).

5. The grating surface is a perfect conductor. This is a good approximation for all metals in the wavelength region covered in the present experiments (18 to 2649 μm).

The reconstruction of the time profile of the bunch is based on the Kramers-Kronig (KK) method for the recovery of the minimal phase. The details and limitations of this method are well documented [11–13] and will not be reviewed here. The basic issue is that measurements of the radiated energy can only provide information about the magnitude (ρ) of the Fourier Transform (FT) of the time profile, but not its phase. From the known magnitude (ρ), the KK method calculates the minimal phase which may differ from the true phase due to the possible existence of additional contributions, the so-called Blaschke phases. These cannot be known a priori.

The application of the KK method requires knowledge of ρ over all frequencies. Our experimental setup allows the simultaneous measurement at eleven frequencies, from a single grating; the use of three different gratings, with suitably chosen periods, extends the range of measured frequencies and improves the accuracy of the reconstruction. In order to calculate the minimal phase, the measured values of ρ (a maximum of 33) were used to create a bigger 1500-point table of ρ vs frequency. This was done by interpolation between the measured values of ρ in the frequency range covered by the experiment and by extrapolation to lower and higher frequencies. The functions used for the extrapolations are important, especially for the low frequencies, which are crucial for the accurate determination of the overall bunch length. Hence, it is desirable to have actually measured points at as low a frequency as practicable. In our experiments the lowest measured frequency ($\nu_{\min}$) was 0.17 THz ($\lambda = 1766$ μm) in June 2012 and 0.113 THz ($\lambda = 2649$ μm) in April 2013. The extrapolation to zero frequency was done by a function of the form $\rho = \rho_0 \exp[-\alpha(\nu - \nu_{\min})^2]$. The quantity ρ_0 is the measured value of ρ at $\nu_{\min}$ and the coefficient α was determined so as to ensure that $\rho \to 1$ when $\nu \to 0$. It was observed that occasionally at the lowest frequencies, generated by the 1.5 mm grating, it was possible to recover ρ values >1. These unphysical values indicate that, within the accuracy of the experiment, the corresponding wavelengths were already longer than the bunch length. In these circumstances, we started the extrapolation not from the lowest measured frequency but from the lowest frequency with $\rho < 1$; all the ρ values at frequencies lower than the start frequency were either set equal to 1 or were replaced by the values given by the extrapolation function. This choice was found to have a very small effect on the reconstructed bunch profile.

For the high frequency extrapolation two different functions were used: (a) a 4th degree polynomial of the form $\rho = \rho_h(\frac{\nu_{\max}}{\nu})^4 + \alpha[(\frac{\nu_{\max}}{\nu})^3 - (\frac{\nu_{\max}}{\nu})^2]$ which matches the value ρ_h at the highest measured frequency ($\nu_{\max}$) and decays asymptotically to zero as $\nu \to \infty$; the coefficient a was adjusted so that the function matched at $\nu_{\max}$ the average slope of the three highest frequency measured points. (b) A simple Gaussian, peaked at $\nu_{\max}$ and whose rate of decay to zero as $\nu \to \infty$ could be adjusted. The choice between these two functions had minimal influence on the bunch profile. All high frequency extrapolations presented here were done with the 4th degree polynomial. The frequency "step" used to create the table was selected so that the table extended from zero frequency to at least 2–3 times the highest measured frequency.

B. Transmission factors and uncertainty estimates

The quantity that is measured during the experiment is $(\frac{dI}{d\Omega})_{N_e}$ i.e., the left-hand side of Eq. (5). The analysis code carries out the calculation of the single-electron yield and then recovers ρ, having taken into account the assumed acceptance of the optical system. However, before this can be done, the signals recorded by the detectors have to be corrected for the losses incurred between the grating and the detectors. These losses, or transmission factors, are due to: (a) the Si window, (b) the filter, (c) the 90° bend, (d) the Winston cone, (e) the detector responsivity, and (f) interference effects. Their combined effect is that, typically, less than 10% of the emitted radiation at the longer wavelengths reaches the pyroelectric detector; at wavelengths shorter than about 100 μm this figure is further reduced because of interference effects.

The measurements reported in this paper carry significant systematic experimental uncertainties. Since the reconstruction of the bunch profile is based on the measurement of the spectral yield by an array of 11

detectors, it is essential to know the responsivities of these detectors in the wavelength band in which they are operating. Based on the work reported in [14,15] we estimate the uncertainty of the detectors' response to be ±50%. The other systematic uncertainties are comparatively small and, therefore, we have assumed a total uncertainty of ∼50% for all the measurements reported here. This refers to the measured values of radiated energy, which are proportional to the square of the FT of the bunch profile; the uncertainty in the recovered values of ρ is half of that, i.e., 25%.

Manifestly, the reconstructed profile also depends on the value of the single-electron yield and, thus, on the physical model used to describe SP radiation. A comparison between the model-dependent single-electron yields is beyond the scope of this paper but we note that, ultimately, the reconstructed profile must be in broad agreement with the expected bunch length, which is known to a good approximation in most accelerator installations and that the measured yields must be in line with the theoretical predictions. This is certainly the case in our experiments (see also the following section).

Clearly a significant improvement can only be achieved by an accurate determination of the relative detector responsivities. This, in turn, would allow a better understanding of any inadequacies in the theory. The details of the various transmission factors and the associated uncertainties are given in the Appendix.

IV. BACKGROUND AND POLARIZATION ISSUES

A. Background radiation

The detection of cSPr depends, amongst other things, on the understanding (and, if possible, suppression) of the background radiation. Since the level of the background is, at least in part, site specific the discussion that follows refers only to our setup at FACET and considers beam-related sources of background radiation. These sources of transition, diffraction or synchrotron radiation could be located upstream or downstream from the grating and the generated radiation could be propagating collinearly with the beam or it could be reaching the detectors having suffered multiple reflections on the way. The grating itself could then disperse any radiation impinging on it. However, according to the theory of gratings [16] and bearing in mind the existence of filters at each observation port, only radiation propagating along the z axis will be dispersed at the correct angle and wavelength so that it can get through the filters. We believe that the contribution of any background radiation propagating along the z axis must be minimal. Instead, the experimental evidence suggests strongly that the dominant contribution is due to radiation scattered from the support structure of the grating, the edge of the grating itself plus radiation that has suffered multiple reflections in the beam pipe and the chamber, before entering the detectors. Our reasoning is as follows: (a) The nearest alternative source of radiation is a Be foil, 2 m away; we have calculated its likely contribution and conclude that it is negligible, at least for the wavelength region covered here. (b) Synchrotron radiation is polarized; had there been a significant intensity of SR propagating collinearly with the beam, we should have seen some evidence of its polarization when inserting the blank. We did not observe this (see Sec. IV B). (c) The upstream apertures are large (of the order of 38 mm) and are unlikely to contribute significantly to diffraction radiation. (d) The measured spectral yields at wavelengths much longer than the bunch length, where the bunch can be treated as one "lump" of charge and the coherence factors tend to unity, are close (better than 1 order of magnitude) to those expected from the reconstructed bunch profile (see Fig. 9 in Sec. V). This would not have been the case if the treatment of the background (or the calculation of the single electron yield) were seriously wrong. Therefore, we are confident that the use of the blank in order to subtract the background contribution is a good approximation, at least for our experimental arrangement. None of the above comments removes the need for careful consideration of the particular circumstances of an experiment or the need for the best possible suppression of the background radiation.

A series of measurements were carried out with the blank and a variety of filters. The aim was to obtain an estimate of the wavelength distribution of the background radiation. The procedure consisted of bringing the blank close to the beam, typically to a distance of between 2.0–2.5 mm, and then inserting one of the filter sets. Only WAP-type filters were used for these measurements. Their transmission curve is characterized by a very sharp cutoff on the long wavelength side and a less steep drop in transmission on the short wavelength side. At very short wavelengths the transmission rises again, extending down to the visible, but the properties in this region have not been measured. For the purposes of the background studies the filters have been treated as high frequency pass filters. This is clearly an approximation because the details of the transmission characteristics at short wavelengths have been ignored. An approximate value for the average transmission was obtained over the wavelength region limited by transmission of less than 20% on the short wavelength side, and <5% on the long wavelength side. The counts obtained in each channel were divided by this average transmission and were then compared with those obtained without the use of any filter. This gives a rough estimate of the fraction of the total background with wavelengths up to the long wavelength cutoff of the filter. It is assumed that the wavelength distribution of the background is uniform over the 11 observation ports.

The results are shown in Fig. 4 where the abscissa is the cutoff wavelength of the filter and the ordinate is the fraction of the total intensity with wavelengths below this

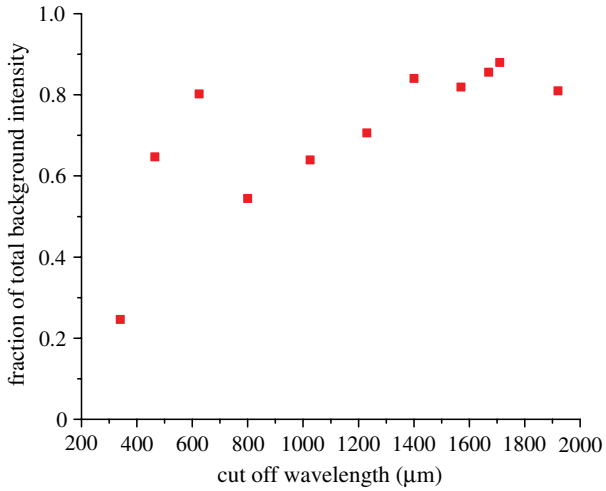

FIG. 4. Approximate wavelength distribution of the background radiation. Note that wavelengths longer than about 2.8 mm cannot be detected by the optical system.

limit. There is some scatter in the results but the general conclusions are: (a) about 25% of the background radiation is in the region 0–350 μm. (b) About 80% of the background is within the region 0–1400 μm, approximately. (c) Opening the transmission window to about 1900 μm causes only a minimal increase in the collected fraction.

We have also carried out "particle-in-cell" (PiC) simulations of the diffraction radiation expected *just from the blank itself* by using the MAGIC code. This is, of course, only one of the sources of background. Its wavelength distribution (Fig. 5) is predominantly in the wavelength region beyond 1.0 mm but these long wavelengths would have been suppressed by the Winston cone (exit aperture = 2.8 mm) and will not appear in Fig. 4. A comparison of Figs. 4 and 5 suggests that the other sources of background must be predominantly high frequency ones, so that the overall background, shown in Fig. 4, is shifted towards shorter wavelengths.

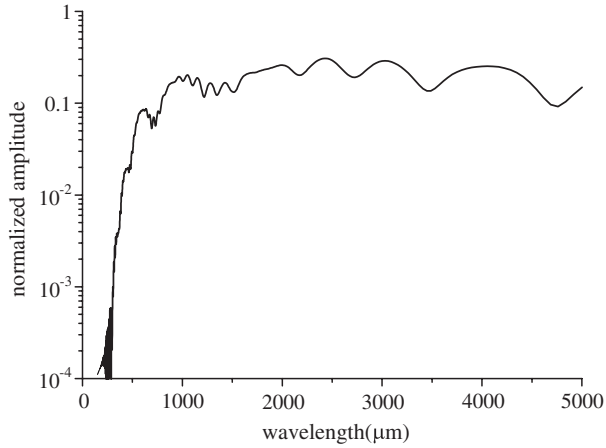

FIG. 5. Particle-in-cell simulation of the diffraction radiation from the leading and trailing edges of the blank grating.

Although these measurements can only provide a broad picture of the wavelength distribution of the background radiation in the FACET area, they are sufficient to confirm that most of the background radiation is below 1400 μm, approximately. This overlaps with the region of the expected cSPr signals and indicates that it is not possible to discriminate against background radiation by filtering alone.

B. Polarization

A limited number of measurements were devoted to the study of the polarization of both the background signal and the Smith-Purcell radiation itself. The purpose of these measurements was to test the theoretical predictions about the degree of polarization of cSPr and to establish if the expected polarization of the cSPr could be used to discriminate it from background. It is important to note that, because the design of the optical system did not allow the simultaneous use of a filter and a polarizer, all polarization measurements were carried out without the use of filters.

The experimental procedure was to replace some of the existing filters with wire polarizers. The polarizers were manufactured by the Rutherford Appleton Laboratory out of Au-coated tungsten wires, 25 μm in diameter and with 64 μm spacing. Their transmission properties have not been measured but they are expected to be similar to those of commercially available polarizers with similar design parameters [17]. For the wavelength range considered here (>200 μm) the transmission for the electric field perpendicular to the wires is expected to be about 99%, while the transmission for the field parallel to the wires is <1%. The polarizers are expected to be "perfect," i.e., no absorption losses in the wires. Since only 18 polarizers were available, no polarizers were placed over the 130° and 140° ports which were thus excluded from these measurements. Half the polarizers were oriented with the wires in the direction of the grating grooves (direction 1) and the other half perpendicular to it (direction 2). The orientation of the polarizer wires was determined by visual inspection. For the determination of the degree of polarization of the background signal, the blank was brought close to the beam (typically between 2.0 and 2.5 mm) and the resulting signal was measured in the two directions. The degree of polarization of the radiation from the blank (p_b) is given by

$$p_b = \frac{B_1 - B_2}{B_1 + B_2}, \tag{6}$$

where B_1 and B_2 are the energies measured with the polarizers in directions 1 and 2, respectively. The two signals were essentially the same, with differences of the order of 3%; this is much lower than the previously mentioned uncertainties in these experiments. Hence, it

is concluded that the background radiation is unpolarized to an accuracy of 3%.

When a grating is used the measured signal (I_i) ($i = 1, 2$) is the sum of the true SP signal (G_i) plus the background (B_i). Therefore, the determination of the degree of polarization of the cSPr requires four separate measurements, two with the grating and another two with the blank. Some trivial manipulations yield the expression for the unknown degree of polarization p_g of the SP signal:

$$p_g \equiv \frac{G_1 - G_2}{G_1 + G_2} = \frac{I_1 - I_2 - p_b(B_1 + B_2)}{I_1 + I_2 - (B_1 + B_2)}. \qquad (7)$$

Equation (7) ignores the fact that, in principle at least, the polarization of the initially unpolarized background radiation could be changed upon diffraction from the surface of the grating. This is due to the different efficiencies of the grating for the s or p polarizations [16]. Whether this is important or not will depend critically on the overall level of the background signal and, specifically, on the component that arrives at the detectors having been diffracted by the grating. There was no way of determining this component with the present experimental setup but we note that the total intensity of the background for this set of data was 20%–30% of that of the cSPr signal, at least for the longer wavelengths. Since the dominant component of the background signal is likely to be scattering from the grating edge and its support structure, it is plausible to assume that the additional error introduced by ignoring this effect is small (compared with the overall experimental uncertainties). The significance of this effect can be reduced through the use of filters. Moreover, the absence of filters means that all wavelengths up to the cutoff the Winston cones (~2.8 mm) can pass through to the detector and the subtraction of the blank signal from that of the grating does not necessarily yield the true SP signal because the resultant difference may still have a significant content of background radiation. The measured degree of polarization is thus a combination of the polarizations of the SP signal and of the background. This is shown in Fig. 6 (upper abscissa) as a function of the observation angle θ for a grating with a period of 1.0 mm. Also shown, for comparison purposes, is the predicted degree of polarization of cSPr originating from a grating of this period and having a width of 20 mm, as a function of wavelength (solid line, lower abscissa).

The measured points indicate that the grating signal is polarized, with polarization that seems to be in agreement with the predictions for wavelengths over 600 μm, approximately; however, the error bars are significant and there is clear lack of agreement at the small observation angles (shorter wavelengths). These measurements are inconclusive and will be repeated with a suitably modified optical system that would allow the simultaneous use of filters and polarizers.

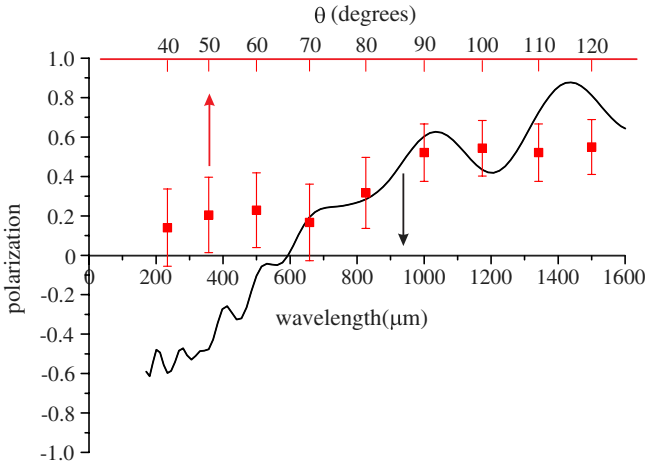

FIG. 6. The measured degree of polarization of the grating signal as a function of observation angle. The solid line is the theoretically predicted polarization of cSPr from the 1.0 mm grating, as a function of wavelength.

The systematic uncertainties in these measurements are due to variations in the beam-grating spacing and to uncertainties in transmission losses and polarizer orientations. It is to be noted that the measurements are not affected by the detector responsivity uncertainty because the same detector is used for both polarization orientations. We estimate that the combined effect of these factors is an uncertainty of $\pm 10\%$ for each measurement. Since the determination of G_1 or G_2 is the difference between two separate measurements, one with the grating and the other with the blank, the uncertainty in G_1 or G_2 must be $\pm 20\%$. The resultant uncertainty in the degree of polarization is indicated by the error bars of the plot. A reduction of the systematic uncertainties can be achieved by the simultaneous measurement of I_1 and I_2. Any statistical uncertainties have been ignored.

V. RECONSTRUCTED PROFILES

The bunch profiles were reconstructed by the superposition of three sets of "grating minus blank" measurements, i.e., six separate runs, each run consisting of about 100 bunches. Care was taken to ensure that the beam-grating separation was the same for each grating-blank pair. Outputs from different gratings were scaled quadratically with charge, after the subtraction of the blank signal.

The averaged net counts were then divided by the overall transmission efficiency for that specific observation channel and were translated into energy by the DAQ calibration factor (35 pJ/count). Net counts below 10 were excluded from the analysis. Division by the solid angle subtended by the cone (~6.4 msr) gives the quantity $\left(\frac{dI}{d\Omega}\right)_{N_e}$ from which ρ^2 can be determined [see Eq. (5)]. The procedure was repeated for the other two grating-blank combinations and the resultant values of ρ were used for the creation of the previously mentioned ρ vs frequency table and the

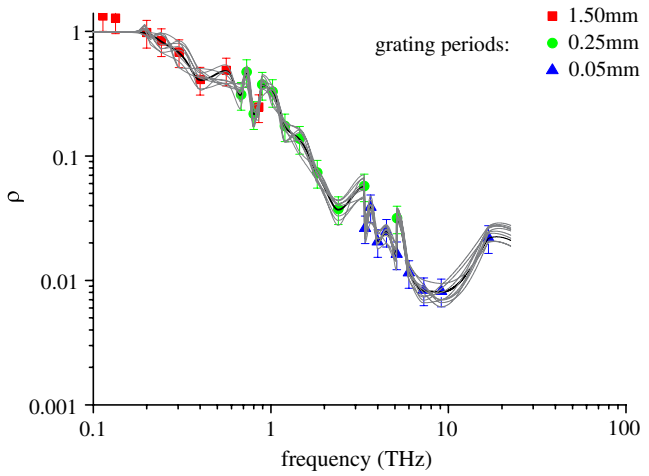

FIG. 7. The magnitude (ρ) of the FT of the time profile of the bunch for a "high compression" run on the April 9, 2013.

subsequent reconstruction of the profile. Figure 7 shows the ρ values, which were derived from three gratings, for a high compression run on April 9, 2013 together with the interpolating/extrapolating curves. Figure 8 shows the time profile recovered from these values. The bold line in Fig. 8 is the profile corresponding to the central values of ρ and the faint lines are the profiles corresponding to random variations of $\pm 25\%$ in these values. The charge was 7.4–7.7 $\times 10^9$ electrons per bunch, and the beam-grating separations were 1.54, 1.53, and 1.28 mm for the 1.5, 0.25, and 0.05 mm gratings, respectively. Due to mechanical damage to three of the very short wavelength filters, the shortest wavelength that could be measured reliably was in the region of 40 μm; thus, it was not possible to exploit fully the range of wavelengths offered by that particular grating which, normally, should have extended down to 12 μm.

It is worth noting that for wavelengths much longer than the bunch dimensions the radiation tends to full coherence and the details of the bunch structure cease to be important; therefore, the measured yields in this region are a good indication of the validity of the calculated single-electron yield. For the FACET bunches and experimental conditions

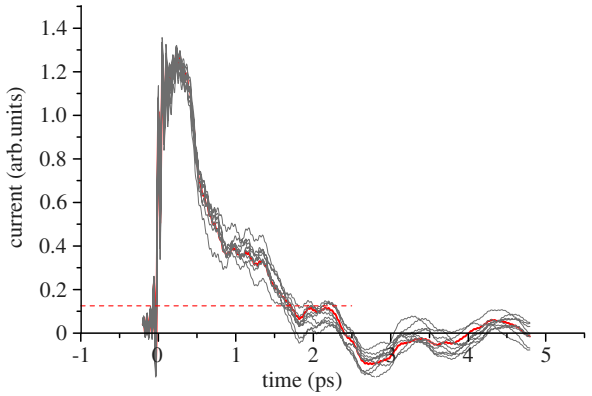

FIG. 8. The bunch profiles corresponding to the data of Fig. 7.

this implies wavelengths >1.0 mm, approximately. The points of Fig. 9 show the measured spectral yields from the three gratings for the run of Fig. 8. The solid lines are the theoretically expected values, based on the profile of Fig. 8. In the long wavelength region (>1.0 mm approximately) the measured values are close (better than an order of magnitude) to those expected from the surface current theory. Given all the uncertainties about measurements in the far infrared, this can be considered acceptable, thus providing good supporting evidence both for the theoretical model of the emission process and for the treatment of the background radiation.

The bunch lengths mentioned in this paper are their weighted rms values:

$$t_{\mathrm{rms}} = \sqrt{\frac{\sum [t^2 * I(t)]}{\sum I(t)} - \left(\frac{\sum [t * I(t)]}{\sum I(t)}\right)^2},$$

where I(t) is the amplitude of the profile at time t. Only points that are higher than 10% of the profile peak (dashed line in Fig. 8) were used in this calculation. Any oscillations in the profile beyond the first "dip" below the 10% level have been ignored; negative oscillations are unphysical and are an artifact of the reconstruction process. The same comment applies to the rapid oscillations of the bunch profile near $t = 0$ (Figs. 8 and 10). The maximum and minimum rms values for this run were 479 and 391 fs, respectively, and the mean was 436 fs. The effects of the uncertainty in ρ are particularly noticeable the trailing end of the bunch. Figure 10 shows the profiles corresponding to a medium compression setting of the accelerator, again on April 9, 2013. The charge for this run was 7.5–7.6 $\times 10^9$ electrons per bunch, and the beam-grating separations were

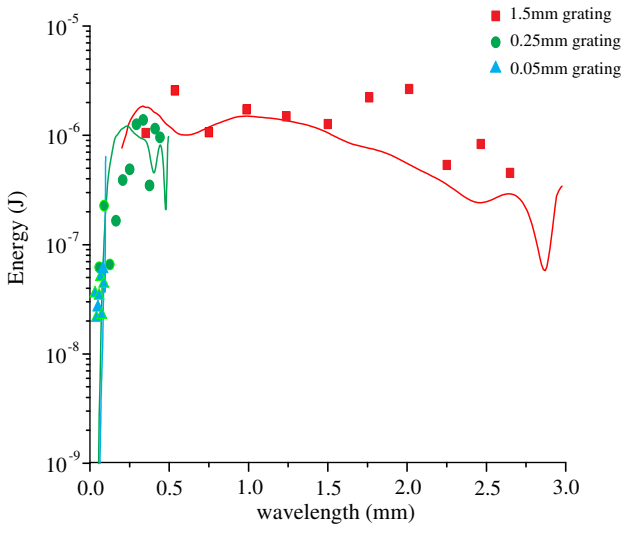

FIG. 9. The measured spectral yield for the run of Fig. 7. The solid lines are the expected yields from each of the three gratings, assuming that the bunch profile is the one shown in Fig. 8.

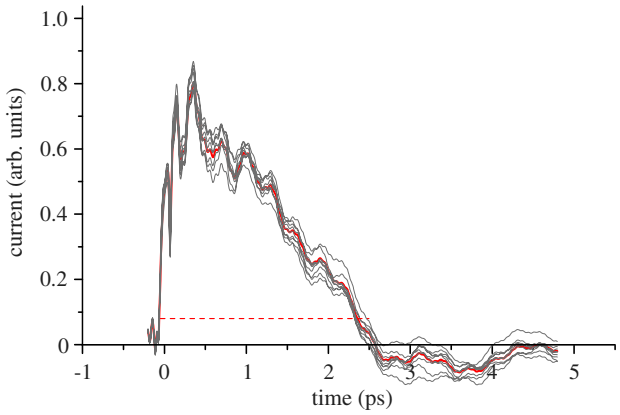

FIG. 10. Bunch profile during a "medium compression" run (April 9, 2013).

1.1, 1.1, and 1.21 mm for the 1.5, 0.25, and 0.05 mm gratings, respectively. The maximum and minimum rms values were 652 and 583 fs, respectively, and the mean value was 604 fs. A limited amount of smoothing has been applied to the leading edge of the profiles but this has no effect on the rms values.

The effect of the systematic uncertainty in the beam-grating separation (± 0.5 mm) on the reconstructed profile is shown in Fig. 11 which is based on the same data set as the profile of Fig. 7. The three profiles correspond to: (a) the nominal separation, determined according to the procedure of Sec. II A (black line), (b) nominal plus 0.5 mm (red line), and (c) nominal minus 0.5 mm (blue line). The corresponding rms values of the bunch length are 437, 405, and 467 fs, respectively. The change in the shape of the profile is small but the change in the bunch length is significant. Possible variations of the beam-grating/blank separation that might occur between a grating run and the corresponding blank one have not been studied but are expected to cause significant variations of the reconstructed profile.

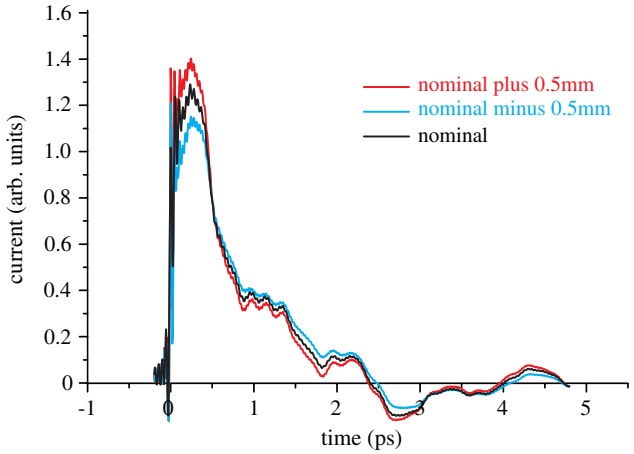

FIG. 11. The data of Fig. 7 plotted for three different values of the beam-grating separation.

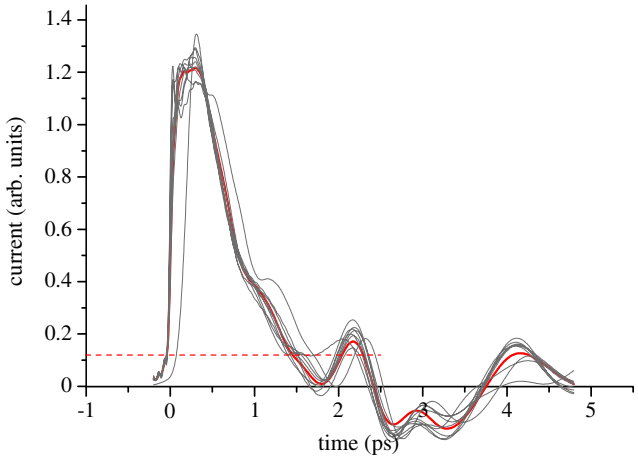

FIG. 12. A set of bunch profiles reconstructed from data taken on June 25, 2012.

The experiments of June 2012 employed gratings with periods of 1.0, 0.5, and 0.25 mm. An example of the bunch profile for a "high compression" run on June 25, 2012 is shown in Fig. 12. The average value of the rms length was 356 fs and the maximum and minimum ones 379 and 328 fs, respectively. The charge for this run was 1.9×10^{10} electrons per bunch and the beam-grating separations were 2.1, 2.4, and 2.4 mm for the 1.0, 0.5, and 0.25 mm gratings, respectively.

VI. SUMMARY AND CONCLUSIONS

The time profiles of a number of sub-ps long bunches, corresponding to different compression settings of the accelerator, have been determined at the FACET facility at SLAC by means of cSPr. The measurements reported here were carried out in 2012 and 2013 and are an extension of the first results reported in [18].

It is worth emphasizing the importance of information about the radiated energy at long wavelengths (low frequencies) because it is precisely these frequencies that are essential for the determination of the bunch length. The lowest measured frequencies were 0.113 and 0.17 THz in 2013 and 2012, respectively, and the required extrapolation to zero frequency was always carried out from that frequency. Therefore, the profiles presented here contain information over a "time window," of the order of 4–5 ps.

Information about the yield at very short wavelengths (high frequencies) is also important because the information about any fine structure inside the profile will be contained in these wavelengths. The shortest wavelength that can potentially be generated by cSPr is that at the most forward observation angle and with the shortest period grating; in these experiments this was about 60 μm ($\sim$200 fs) in 2012 and 40 μm ($\sim$130 fs) in 2013. Therefore, any details of the time profile that might be finer than these figures would not have been measurable.

The detection of short wavelengths is particularly sensitive to the beam-grating separation, the reason being that the coupling efficiency follows, approximately, the exponential dependence of Eq. (2a) although this is strictly true only for gratings of infinite width. Good coupling requires small beam-grating separation x_0 and/or long evanescent wavelength λ_e [Eq. (3)]. Note that because of the fact that any optical system will accept rays over a finite range of azimuthal angles ϕ, $\sin\phi \neq 0$ in Eq. (3). The azimuthal range collected by our Winston cones is $|\phi| = 0$–$3°$.

An important feature of any Smith-Purcell experiment is the inevitable presence of radiation that does not originate from the grating itself. This has been referred to in this paper as "background radiation" and it is evident that the cSPr signal must be at least as big as the background before it can be detected. The magnitude and properties of the background will depend on the specific experimental arrangement. At FACET the level of the background signal was of the order of 10^{-8} J, which is about a factor of 5–10 higher than previous experiments at ESA [7]. We have measured its wavelength distribution in the far infrared part of the spectrum and established that it lies primarily in the wavelength region between 600–1700 μm, approximately. This overlaps with the expected range of cSPr wavelengths. Because of the size of its exit diameter, wavelengths greater than 2.8 mm are suppressed by the Winston cone. It has also been established that the background radiation is essentially unpolarized. The SP radiation itself was found to be polarized but the attempt to measure its degree of polarization was inconclusive because the design of the experiment was not optimized for this type of measurement. There have been, to our knowledge, very few measurements [19] of this important parameter which is inherently interesting and potentially important in simplifying the design of a future single-shot device.

The main conclusions from this work are: (a) at the high compression setting of the accelerator, the main part of the bunch is contained within 1 ps but there is a trailing part that extends beyond this time. (b) Taking that into account, the weighted rms length of various compressed bunches was found to be ~436 fs and ~356 fs in 2013 and 2012, respectively. (c) For the medium compression setting, the rms length (2013 data) was ~604 fs. (d) The ±0.5 mm uncertainty in the beam-grating separation introduces an uncertainty of ±7% in the rms value of the bunch length. (e) An uncertainty of similar magnitude is introduced by the lack of accurate information about the relative responsivities of the eleven pyroelectric detectors. A new set of calibration checks is being planned in order to address this point.

As a general comment, we note that a diagnostic device based on cSPr has to be considered as part of a suite of diagnostic devices such as BPMs and charge monitors. This would allow an accurate measurement of the charge and of the beam-grating separation, both of which are crucial parameters for the reconstruction of the profile, especially for very short bunches.

ACKNOWLEDGMENTS

The authors are grateful to Peter Lau of the Oxford Design Office and to the Oxford and LAL workshops for their skill and efficiency in the design and manufacture of the mechanical components of the system. The financial support of the John Adams Institute, the Fell Fund (University of Oxford), the IN2P3 and the Université Paris-Sud (program "attractivité") and the French ANR (Contract No. ANR-12-JS05-0003-01) are gratefully acknowledged. The Valencia group have been supported by Contracts No. IDC-20101074 and No. FPA2010-21456-C02-01. We have profited from numerous discussions with Professor Alan Fisher of Stanford University and Dr. Peter Huggard of Rutherford Appleton Laboratory. This work was performed (in part) under DOE Contract No. DE-AC02-7600515.

APPENDIX

See Table I.

TABLE I. Transmission factors for each element of the optical system and their uncertainties. The tabulation is presented as a function of the observation angle θ and the corresponding wavelength, for each grating used in these experiments.

θ (deg)	Grating period (μm)	λ (μm)	Si window[a]	Filter ±10%[b]	Elbow ±5%[c]	Cone ±5%[d]	Detector relative responsivity ±50%[e]	Far-field ±5%[f]	Total ±50%
40	50	12 ± 2	0.42	0.25	0.80	0.465	0.80	0.150	0.005
	250	58 ± 8	0.50	0.30	0.80	0.465	0.80	0.353	0.016
	500	117 ± 17	0.55	0.62	0.80	0.465	0.80	0.590	0.060
	1000	234 ± 34	0.55	0.59	0.80	0.465	0.80	0.998	0.096
	1500	351 ± 50	0.55	0.30	0.80	0.465	0.80	1.000	0.049
50	50	18 ± 2	0.30	0.13	0.80	0.465	0.77	0.140	0.002
	250	89 ± 10	0.53	0.33	0.80	0.465	0.77	0.485	0.024
	500	179 ± 20	0.55	0.80	0.80	0.465	0.77	0.973	0.123
	1000	357 ± 40	0.55	0.34	0.80	0.465	0.77	0.998	0.053
	1500	536 ± 60	0.55	0.29	0.80	0.465	0.77	1.000	0.046

(Table continued)

TABLE I. (*Continued*)

θ (deg)	Grating period (μm)	λ (μm)	Si window[a]	Filter $\pm 10\%$[b]	Elbow $\pm 5\%$[c]	Cone $\pm 5\%$[d]	Detector relative responsivity $\pm 50\%$[e]	Far-field $\pm 5\%$[f]	Total $\pm 50\%$
60	50	25 ± 2	0.49	0.50	0.80	0.465	1.00	0.193	0.018
	250	125 ± 11	0.54	0.34	0.80	0.465	1.00	0.597	0.041
	500	250 ± 23	0.55	0.40	0.80	0.465	1.00	0.998	0.082
	1000	500 ± 45	0.55	0.34	0.80	0.465	1.00	1.000	0.070
	1500	750 ± 68	0.55	0.82	0.80	0.465	1.00	0.987	0.166
70	50	33 ± 2	0.49	0.61	0.80	0.465	0.75	0.214	0.018
	250	164 ± 12	0.55	0.39	0.80	0.465	0.75	0.816	0.049
	500	329 ± 25	0.55	0.34	0.80	0.465	0.75	0.997	0.052
	1000	658 ± 49	0.55	0.83	0.80	0.465	0.75	0.983	0.125
	1500	987 ± 74	0.55	0.85	0.80	0.465	0.75	1.000	0.130
80	50	41 ± 3	0.50	0.68	0.80	0.465	0.75	0.237	0.022
	250	207 ± 13	0.55	0.51	0.80	0.465	0.75	0.998	0.078
	500	413 ± 26	0.55	0.40	0.80	0.465	0.75	0.991	0.061
	1000	826 ± 52	0.55	0.70	0.80	0.465	0.75	1.000	0.107
	1500	1240 ± 77	0.55	0.90	0.80	0.465	0.75	0.988	0.136
90	50	50 ± 3	0.50	0.55	0.80	0.465	0.83	0.244	0.021
	250	250–13	0.55	0.51	0.80	0.465	0.83	0.998	0.086
	500	500 ± 26	0.55	0.40	0.80	0.465	0.83	1.000	0.068
	1000	1000 ± 52	0.55	0.75	0.80	0.465	0.83	1.000	0.127
	1500	1500 ± 78	0.55	0.68	0.80	0.465	0.83	0.973	0.112
100	50	59 ± 3	0.50	0.57	0.80	0.465	0.62	0.375	0.025
	250	293 ± 13	0.55	0.40	0.80	0.465	0.62	0.997	0.051
	500	587 ± 26	0.55	0.37	0.80	0.465	0.62	0.995	0.047
	1000	1174 ± 52	0.55	0.85	0.80	0.465	0.62	0.990	0.107
	1500	1760 ± 77	0.55	0.50	0.80	0.465	0.62	0.968	0.061
110	50	67 ± 2	0.51	0.76	0.80	0.465	0.75	0.423	0.046
	250	335 ± 12	0.55	0.36	0.80	0.465	0.75	0.998	0.055
	500	671 ± 25	0.55	0.36	0.80	0.465	0.75	0.983	0.054
	1000	1342 ± 49	0.55	0.84	0.80	0.465	0.75	0.981	0.126
	1500	2013 ± 74	0.55	0.69	0.80	0.465	0.75	0.971	0.103
120	50	75 ± 2	0.52	0.69	0.80	0.465	1.02	0.443	0.060
	250	375 ± 11	0.55	0.86	0.80	0.465	1.02	0.999	0.179
	500	750 ± 23	0.55	0.82	0.80	0.465	1.02	0.987	0.169
	1000	1500 ± 45	0.55	0.76	0.80	0.465	1.02	0.974	0.154
	1500	2250 ± 68	0.55	0.72	0.80	0.435	1.02	0.970	0.136
130	50	82 ± 2	0.52	0.70	0.80	0.465	0.86	0.483	0.056
	250	411 ± 10	0.55	0.40	0.80	0.465	0.86	0.991	0.070
	500	821 ± 20	0.55	0.67	0.80	0.465	0.86	0.996	0.117
	1000	1642 ± 40	0.55	0.40	0.80	0.465	0.86	0.972	0.068
	1500	2464 ± 60	0.55	0.75	0.80	0.308	0.86	0.973	0.085
140	50	88 ± 2	0.53	0.79	0.80	0.465	0.70	0.552	0.060
	250	442 ± 8	0.55	0.40	0.80	0.465	0.70	0.990	0.057
	500	883 ± 17	0.55	0.55	0.80	0.465	0.70	1.000	0.079
	1000	1766 ± 34	0.55	0.53	0.80	0.465	0.70	0.969	0.074
	1500	2649 ± 50	0.55	0.78	0.80	0.292	0.70	0.980	0.069

[a]Manufacturer's data.
[b]Measured.
[c]Best estimate.
[d]Measured. This number is determined by the concentration factor of the cone, the detector diameter and the separation between detector and cone exit. See also Ref. [7].
[e]Measured. These are relative values, compared to that of an arbitrarily chosen "reference" detector. The absolute responsivity was taken from the manufacturer's data.
[f]Calculated.

[1] J. Faure, Y. Glinec, A. Pukhov, S. Kiselev, S. Gordienko, E. Lefebvre, J.-P. Rousseau, F. Burgy, and V. Malka, Nature (London) **431**, 541 (2004).
[2] W. P. Leemans, B. Nagler, A. J. Gonsalves, Cs. Tóth, K. Nakamura, C. G. R. Geddes, E. Esarey, C. B. Schroeder, and S. M. Hooker, Nat. Phys. **2**, 696 (2006).
[3] I. Blumenfeld, C. E. Clayton, F. J Decker, M. J. Hogan, C. Huang, R. Ischebeck, R. Iverson, C. Joshi, T. Katsouleas, N. Kirby, W. Lu, K. A. Marsh, W. B. Mori, P. Muggli, E. Oz, R. H. Siemann, D. Walz, and M. Zhou, Nature (London) **445**, 741 (2007).
[4] A. D. Debus *et al.*, Phys. Rev. Lett. **104**, 084802 (2010).
[5] S. Wesch, B. Schmidt, C. Behrens, H. Delsim-Hashemi, and P. Schmüser, Nucl. Instrum. Methods Phys. Res., Sect. A **665**, 40 (2011).
[6] D. V. Karlovets and A. P. Potylitsyn, Phys. Rev. ST Accel. Beams **9**, 080701 (2006).
[7] V. Blackmore, G. Doucas, C. Perry, B. Ottewell, M. Kimmitt, M. Woods, S. Molloy, and R. Arnold, Phys. Rev. ST Accel. Beams **12**, 032803 (2009).
[8] A. S. Kesar, Phys. Rev. ST Accel. Beams **13**, 022804 (2010).
[9] J. H. Brownell, J. Walsh, and G. Doucas, Phys. Rev. E **57**, 1075 (1998).
[10] S. R. Trotz, J. H. Brownell, J. Walsh, and G. Doucas, Phys. Rev. E **61**, 7057 (2000).
[11] O. Grimm and P. Schmüser, TESLA FEL Report No. 2006-03.
[12] R. Lai and A. J. Sievers, Phys. Rev. E **50**, R3342 (1994).
[13] L. Frölich, TESLA-FEL Report No. 2005-02.
[14] V. Blackmore, D.Phil. thesis, University of Oxford, 2008.
[15] R. Guillemet, University of Oxford, Department of Physics Report, 2011.
[16] E. G. Loewen, M. Nevière, and D. Maystre, Appl. Opt. **16**, 2711 (1977).
[17] P. Huggard (private communication).
[18] R. Bartolini, C. Clarke, N. Delerue, G. Doucas,, and A. Reichold, JINST **7**, P01009 (2012).
[19] Y. Shibata, S. Hasebe, K. Ishi, S. Ono, M. Ikezawa, T. Nakazato, M. Oyamada, S. Urasawa, T. Takahashi, T. Matsuyama, K. Kobayashi, and Y. Fujita, Phys. Rev. E **57**, 1061 (1998).